



Full Text View

[Volume 30, Issue 9 \(September 2000\)](#)

Journal of Physical Oceanography

Article: pp. 2439–2451 | [Abstract](#) | [PDF \(416K\)](#)

Comparison of Two Classical Advection Schemes in a General Circulation Model

Yasuhiro Yamanaka^{*}, Ryo Furue, Hiroyasu Hasumi, and Nobuo Suginozohara

Center for Climate System Research, University of Tokyo, Tokyo, Japan

(Manuscript received September 29, 1997, in final form February 24, 2000)

DOI: 10.1175/1520-0485(2000)030<2439:COTCAS>2.0.CO;2

ABSTRACT

The authors compare two classical advection schemes, the centered difference and weighted upcurrent, for coarse-resolution OGCMs, using an idealized ocean basin and a realistic World Ocean topography. For the idealized basin, three experiments are run, one with 12 vertical levels and the centered difference scheme, one with 12 levels and the weighted upcurrent scheme, and the other with 800 levels and the centered scheme. The last experiment perfectly satisfies the grid Péclet number stability criterion and is regarded as the “true solution.” Comparison of the coarse vertical resolution experiments with the true solution indicates 1) that with the centered scheme, when strong vertical motion crosses a strong stratification, false density values are created in the coarse resolution model and this leads to false convective adjustment, which transports those false density values downward; and 2) that because of computational diffusion, the weighted upcurrent scheme leads to a less dense deep water with a stronger stratification than those of the true solution. These characteristics also apply even to the World Ocean model with relatively small grid Péclet numbers (moderately high vertical resolution and relatively large vertical diffusivity): the centered scheme leads to artificial convective adjustment near the surface in the equatorial Pacific, creating an artificial circulation, and the weighted upcurrent scheme leads to a warmer deep water and more diffuse thermocline. Deep equatorial “stacked jets” are found in all idealized-basin experiments, in particular, in the super-high vertical resolution case. Horizontal diffusion is found to dominate the density balance at the bottom jet in the super-high-resolution model, as previously found in an OGCM with a moderately high vertical resolution. This is consistent with the hypothesis that the jets exist owing to diapycnal mixing.

Table of Contents:

- [Introduction](#)
- [Idealized basin ocean](#)
- [World Ocean](#)
- [Summary](#)
- [REFERENCES](#)
- [TABLES](#)
- [FIGURES](#)

Options:

- [Create Reference](#)
- [Email this Article](#)
- [Add to MyArchive](#)
- [Search AMS Glossary](#)

Search CrossRef for:

- [Articles Citing This Article](#)

Search Google Scholar for:

- [Yasuhiro Yamanaka](#)
- [Ryo Furue](#)
- [Hiroyasu Hasumi](#)
- [Nobuo Suginozohara](#)

1. Introduction

The two classical advection schemes, the centered difference and upcurrent, are widely used in ocean general circulation models (OGCMs). For example, the GFDL Modular Ocean Model adopts the centered difference (e.g., [Toggweiler et al. 1989](#); [Najjar et al. 1992](#)), and the Hamburg LSG model adopts the upcurrent (e.g., [Bacastow and Maier-Reimer 1990](#); [Maier-Reimer et al. 1993](#)) scheme. The weighted upcurrent scheme, which is a combination of the upcurrent and centered difference schemes, is also used (e.g., [Suginohara and Fukasawa 1988](#); [Yamanaka and Tajika 1996](#)). Numerical problems of these advection schemes are well known (e.g., [Rood 1987](#)): the centered difference scheme can cause numerical instability while it is free from computational diffusion; the upcurrent scheme brings about computational diffusion but does not cause numerical instability.

[Suginohara and Fukasawa \(1988\)](#) and [Suginohara and Aoki \(1991\)](#) found stacked jets, vertically alternating zonal flows, at the equator in their OGCM with the weighted upcurrent scheme. [Weaver and Sarachik \(1990\)](#) argued that numerical instability of the advection scheme is the cause of the jets. This led to a discussion between these authors about numerical stability of the two advection schemes ([Suginohara et al. 1991](#); [Weaver and Sarachik 1991](#)). More recently, [Wang \(1995\)](#) demonstrated that the stacked jets are not computational but due to diapycnal diffusion arising from the large lateral diffusivity. In this note we confirm Wang's conclusion, using an OGCM with a super-high vertical resolution.

The error associated with weighted upcurrent differencing for the vertical advection term in the temperature equation can be written as

$$\frac{\partial}{\partial z} \left[\left(\alpha - \frac{1}{2} \right) |w| \Delta Z \frac{\partial T}{\partial z} \right] + O(\Delta Z^2), \quad (1)$$

where w is the vertical velocity, ΔZ the vertical grid size, and α the upcurrent weight ([Furue et al. 1995](#)). The weighted upcurrent scheme is a combination of the centered and pure upcurrent schemes in that, when $\alpha = 1$, it is the pure upcurrent scheme and, when $\alpha = 1/2$, it is the centered scheme. [Equation \(1\)](#) indicates that the vertical computational diffusion coefficient is

$$A_{\text{comp}} \equiv \left(\alpha - \frac{1}{2} \right) |w| \Delta Z. \quad (2)$$

The vertical grid Péclet number is defined as

$$\text{Pe} \equiv \frac{(1 - \alpha) |w| \Delta Z}{A_{\text{HV}}}, \quad (3)$$

where A_{HV} is the coefficient of explicit vertical diffusion. The grid Péclet number must be less than unity to keep the scheme numerically stable (e.g., [Bryan 1989](#)). This criterion is relevant only for the vertical direction of tracer equations. The derivation of the criterion assumes a one-dimensional balance between the advection and diffusion terms ([Bryan 1989](#)). Such a balance generally holds for tracers in the vertical (e.g., [Suginohara and Aoki 1991](#)), but not in the horizontal directions or for the momentum equation.

The pure upcurrent scheme is absolutely numerically stable because $\text{Pe} = 0$ for $\alpha = 1$, although computational diffusion can be large. On the other hand, the centered difference is free from computational diffusion, although it is conditionally numerically unstable. When the grid Péclet number criterion is violated, a false tracer value can be created. For example, consider an idealized situation where there is a horizontally uniform stable density stratification with density ρ_1 at vertical level 1 and ρ_2 at level 2 below. Further suppose that at some horizontal location, the vertical velocity w is upward between the two levels and is vanishing above level 1 and below level 2 so that there is horizontal convergence at level 2 and divergence at level 1. When $\text{Pe} > 1$, advection evaluated with the centered-difference scheme may produce a density value larger than ρ_2 at level 2. This value can be larger than the density of the level below level 2. This density inversion can lead to eventual instability and model breakdown, but in a typical OGCM, convective adjustment erases the density inversion and allows stable integration. Even in this case, the suppressed instability can affect the result of the calculation in undesirable ways. For instance, false tracer values may affect the global circulation as will be seen later. Also, convective adjustment leads to large vertical mixing, which can be far larger than the mixing by computational diffusion associated with the upcurrent scheme. This can partly offset the advantage of the centered difference scheme in its freedom from computational diffusion. We call this convective adjustment “artificial” convective adjustment because it is switched on by a false or artificial density inversion. The weighted upcurrent scheme is a trade-off between the pure upcurrent and centered schemes.

It is an attempt to keep computational diffusion as small as possible and at the same time to prevent false tracer values and resultant artificial convective adjustment.

In this study, we compare the centered difference and upcurrent schemes. First, we run an OGCM with a super-high vertical resolution of 800 levels in an idealized ocean basin. In this run, the grid Péclet number criterion is everywhere satisfied. Using this result as a reference, we compare results of OGCMs with a typical vertical resolution to assess merits and pitfalls of the two schemes. Next, we compare the two schemes as applied to an OGCM with a realistic World Ocean bathymetry.

The next section presents results for the idealized-basin model, and [section 3](#), for the realistic World Ocean model. Finally, [section 4](#) summarizes this note.


2. Idealized basin ocean

a. Model and experimental design

We use version 1 of the Center for Climate System Research ocean general circulation model (CCSR-OGCM; [Yamanaka and Tajika 1996](#)), which is based on the model that [Suginohara and Fukasawa \(1988\)](#) and [Suginohara and Aoki \(1991\)](#) used. The model domain is a rectangle with a constant depth of 4000 m on an equatorial β plane, whose longitudinal and latitudinal widths are respectively 3000 and 6000 km. The equator is located at the center of the basin. The configuration of forcing is the same as that of [Suginohara and Fukasawa \(1988\)](#): internal body cooling with a constant reference density at the southwest corner below the depth of about 1000 m and uniform heating with a constant reference density at the sea surface. We, however, alter some of the forcing parameters to obtain a much weaker flow. The cooling and heating reference densities are $27 \sigma_\theta$ and $24 \sigma_\theta$. The density difference, $3 \sigma_\theta$, is smaller than that of Suginohara and Fukasawa. We remove the plateau region from the horizontal distribution of the body cooling coefficient, which now begins to decay from the western boundary. The resultant coefficient is smaller than that of Suginohara and Fukasawa. Also, we remove the density flux through the southern boundary.

This model configuration and forcing are chosen to yield very weak circulation so as to maintain $Pe < 1$ everywhere in the super-high resolution model. In particular, we choose body cooling for this purpose because surface differential cooling would induce strong meridional flow ([Suginohara and Aoki 1991](#)), which would result in strong upwelling and downwelling at lateral boundaries. Later in this section we will discuss supplementary experiments with surface differential cooling rather than body cooling. The stratification will be also weak in the present body-cooling experiments.

The coefficients of horizontal and vertical diffusion are $A_{HH} = 1 \times 10^3 \text{ m}^2 \text{ s}^{-1}$ and $A_{HV} = 1 \times 10^{-4} \text{ m}^2 \text{ s}^{-1}$, and those of horizontal and vertical viscosity are $A_{MH} = 8 \times 10^3 \text{ m}^2 \text{ s}^{-1}$ and $A_{MV} = 1 \times 10^{-4} \text{ m}^2 \text{ s}^{-1}$. The meridional gradient of the Coriolis parameter β is $2 \times 10^{-11} \text{ m}^{-1} \text{ s}^{-1}$. The horizontal grid size is taken to be 100 km to resolve the equatorial radius of deformation for higher vertical modes, as the stacked jets consist of many vertical higher modes ([Suginohara and Aoki 1991](#); [Furue et al. 1995](#)).

We carry out three experiments ([Table 1](#) ): 800 levels with the centered difference (expt I), 12 levels with the centered difference (expt II), and 12 levels with the weighted upcurrent scheme (expt III). For the 800-level model, the vertical grid size is constant from the sea surface to the bottom. The level thicknesses for the 12-level models are respectively 50, 70, 110, 170, 260, 300, and 440 m for the upper seven levels and 520 m for the lower five. For the weighted upcurrent scheme, we use $\alpha = 0.8$ in the horizontal and $\alpha = 1$ (pure upcurrent) in the vertical. Usually we have used $\alpha < 1$ for the vertical, but here we use $\alpha = 1$ for a cleaner comparison.

For expts II and III, the initial condition is a state of no motion and horizontally uniform density stratification. Since we use body cooling, which does not produce any vertical density inversion, convection should not occur. In fact, expt III is run without convective adjustment. However, we use it for expt II because without it false density inversions occur as explained in introduction; the convective adjustment scheme is the same as the “standard scheme” of the GFDL MOM 2 ([Pacanowski 1995](#)) with the number of iterations being one. The ocean has reached a steady state after an integration of about 2000 years in each of expts II and III. In expt I, integration is done for about 2000 years from the steady state of a 40-level model, and the steady state is reached. Convective adjustment is not used. We discuss the final state of integration in all cases.

b. Results and discussion

The horizontal circulation pattern in deep layers is that of [Stommel and Arons \(1960\)](#), as discussed in detail by [Suginohara](#)

and Aoki (1991). In the interior, the maximum vertical velocity is about $4 \times 10^{-7} \text{ m s}^{-1}$ in expts I and III, and $5 \times 10^{-7} \text{ m s}^{-1}$ in expt II; these values occur at the depth of roughly 2000 m in all experiments. Consequently, the maximum grid Péclet number in the interior is far less than unity in expt I. In expt II, it is slightly greater than unity in a small area of the interior and slightly less than unity in the other part of it. The computational diffusion coefficient in expt III is as large as the explicit diffusivity at these depths. The largest vertical velocity occurs along the southern boundary, the western boundary in the southern hemisphere, and the equator in all experiments. The absolute value of the maximum vertical velocity is $2\text{--}6 (\times 10^{-5} \text{ m s}^{-1})$ along the southern boundary and the western boundary in the southern hemisphere. These maxima occur again at the depth of roughly 2000 m. Within 100 km from the equator and outside the western Munk layer, the maximum vertical velocity is $1\text{--}3 (\times 10^{-6} \text{ m s}^{-1})$ in expt I, $6\text{--}9 (\times 10^{-6} \text{ m s}^{-1})$ in expt II, and $2\text{--}4 (\times 10^{-6} \text{ m s}^{-1})$ in expt III. These maxima occur at the depths of 3000–3500 m.

In expt I, the maximum grid Péclet number is 0.83, and hence this experiment satisfies the grid Péclet number criterion everywhere in the computational domain. We regard the result of this experiment as the “true solution.” In expt II, the maximum grid Péclet number is 1.7×10^2 . The maximum computational diffusion coefficient in expt III is $1.1 \times 10^{-2} \text{ m}^2 \text{ s}^{-1}$.

The left three panels (a–c) of [Fig. 1](#) show the meridional volume transport streamfunction, zonally averaged zonal velocity, and zonally averaged density for expt I. There are stacked jets at the equator in this super-high resolution model, which satisfies the grid Péclet number criterion.

[Figure 2](#) shows the balance in the density equation at $x = 1450 \text{ km}$, $y = -50 \text{ km}$ (the closest density point to the equator). The vertical distribution of each term is extremely similar to [Wang’s \(1995\)](#) result (his Fig. 13b), and the horizontal diffusion and vertical advection terms dominate at the depths of the eastward jet. Numerical instability is, hence, not necessary for the existence of the stacked jets, and the above result is consistent with Wang’s conclusion that the jets are maintained by diapycnal mixing arising from horizontal diffusion.

There is strong upwelling connecting the eastward core of the bottom jet to the westward core above and strong downwelling to the south and north of the jets. This upwelling–downwelling system forms meridional dipole cells ([Suginohara and Aoki 1991](#)). These cells manifest themselves as bends in overturning streamfunction contours from the depth of 3000 m to the bottom near the equator ([Fig. 1a](#)).

The central (d–f) and right (g–i) three panels of [Fig. 1](#) show differences of expts II and III from expt I. In expt II, a complicated change in the streamfunction and zonal velocity is found in the deep-water formation region, where the vertical velocity is largest. This is most likely due to the change in the local density structure, which is in turn caused by false density production along the boundaries. Another large difference is found near the equator. This is due to the change in the strength and vertical structure of the stacked jets. The eastward equatorial jet on the bottom is stronger than that in expt I, and the westward jet above is also stronger and its core is at a deeper depth. Higher mode features are enhanced between the depths of 600 m and the sea surface. The enhancement of the stacked jets is accompanied with that of the equatorial dipole cells ([Fig. 1d](#)). These changes in the strength and structure of the stacked jets may be due to the change in the energy conversion among different vertical modes along the western boundary ([Furue et al. 1995](#)) and this change may be a result of the strong vertical velocity and ensuing artificial convective adjustment. The change in the global density structure (see below) may also contribute to the change in the vertical structure of the equatorial jets.

The zonally averaged density difference is more meridionally uniform ([Fig. 1f](#)) than the difference in the zonally averaged streamfunction and zonal velocity. This difference ($\sim -0.1 \sigma_\theta$ above the depth of 1500 m) may be mostly due to the difference in the vertical representation of the body cooling. In the 800-level model, the restoring coefficient is zero from the sea surface to the depth of 992.5 m and nonzero from 997.5 m to the bottom, the midpoint being 995 m; in the 12-level model, the coefficient is zero to 810 m and nonzero from 1180 m, the midpoint being the same as that of the 800-level model. Using the method of [Ishikawa et al. \(1996\)](#) and [Obata et al. \(1996\)](#), we have estimated that the density difference will be $\sim -0.1 \sigma_\theta$ near the sea surface, $\sim +0.07 \sigma_\theta$ at the depth of about 1000 m, and then nearly zero below 2000 m. Since this estimation roughly coincides with the difference in [Fig. 1f](#) above 1500 m, we cannot meaningfully discuss the possible numerical error and instability associated with the centered difference scheme above 1500 m in [Fig. 1f](#). However, the density below the depth of 1500 m is slightly higher than that in expt I. Although it cannot be seen in [Fig. 1f](#), we find that below the depth of 2200 m, the density is even higher than the reference density of body cooling: the average density for $x = 0$ to 3000 km, $y = -2000$ to 3000 km, and $z = 2500$ to 4000 m is about $27.009 \sigma_\theta$, and the maximum value is about $27.017 \sigma_\theta$, which occurs at $x \approx 50 \text{ km}$, $y \approx 2400 \text{ km}$, and $z \approx 2000 \text{ m}$. When advection and diffusion operate in a physical way, a density value outside $24\text{--}27 \sigma_\theta$ should never occur. The density values higher than $27 \sigma_\theta$ are due to false density production associated with the strong upwelling along the western boundary. As mentioned earlier, vertical velocity maxima occur at the depth of about 2000 m along the western boundary. This produces density values larger than $27 \sigma_\theta$ just below

the vertical velocity maxima. These false density values are brought to the deepest layers by convective adjustment and at the same time are spread all over the deep layers of the whole domain by the spreading of the deep water with the deep western boundary current.

Strong upwelling thus acts as an artificial density source below the depth of maximum upwelling. The strong downwelling near the southern boundary should act as density sink above the depth of maximum downwelling, although the possible density difference arising from this mechanism is masked by the difference due to the difference in the vertical representation of the body cooling, discussed earlier.

In expt III, the meridional overturning circulation becomes much stronger than that of expt I (Fig. 1g). This is due to the large interior computational diffusion mentioned earlier. The stacked jets are much stronger than in expt I (Fig. 1h), and an associated increase of the equatorial dipole cells is recognizable (Fig. 1g). The vertical scale of the stacked jets becomes smaller, which indicates enhancement of higher vertical modes. The density becomes higher above the depth of 1500 m and lower below than that of expt I (Fig. 1i). Also, the density stratification becomes weaker from the thermocline depths to the depths of 2000 m and stronger below 2000 m: the Brunt-Väisälä frequency averaged horizontally from $y = -1500$ km to the northern boundary (not shown) is lower by $0.6-1 (\times 10^{-3} \text{ s}^{-1})$ from 1000 m to 2000 m and higher by $0.2-0.4 (\times 10^{-3} \text{ s}^{-1})$ below 2000 m than that in expt I. These changes in the density structure are again due to the large computational diffusion. The change in the strength and vertical structure of the stacked jets may be due to the enhancement of the thermohaline circulation and to the change in the deep stratification. The latter point is consistent with Obata et al.'s (1996) results that a slight increase in deep stratification tends to lead to a large enhancement of higher vertical modes. Changes in the modal conversion along the western boundary may also contribute.

We have also carried out additional experiments with surface differential cooling rather than internal body cooling. We use version 2 of the CCSR-OGCM (Hasumi and Sugimoto 1999). The model domain is similar to that of the body-cooling experiments, but this model uses spherical coordinates. The domain is a 30° wide sector of the sphere, extending from 30°S to 30°N , with a constant depth of 4000 m. The horizontal resolution is $1^\circ \times 1^\circ$. There are 12 levels in the vertical, with resolution varying from 50 m near the surface to 500 m near the bottom. The coefficients of viscosity and diffusion are the same as those for the body-cooling experiments except $A_{\text{HH}} = 4 \times 10^3 \text{ m}^2 \text{ s}^{-1}$ here. Salinity is held constant at 35 psu everywhere. The sea surface reference temperature is zonally uniform and varies linearly from 2°C at the southernmost gridpoints to 23°C at the equator and then maintains the constant value of 23°C throughout the northern hemisphere. These temperature values respectively correspond to the density values of $28 \sigma_\theta$ and $24 \sigma_\theta$. The restoring time for the uppermost layer is 100 days. The convective adjustment scheme is the standard one of the CCSR-OGCM (Hasumi and Sugimoto 1995).

We have carried out two experiments with the centered difference and weighted upcurrent schemes. In the centered-difference experiment, there is strong upwelling, the maximum speed almost reaching $1 \times 10^{-4} \text{ m s}^{-1}$, along the western boundary in the southern hemisphere, and strong downwelling, the maximum speed being about $0.8 \times 10^{-4} \text{ m s}^{-1}$, along the southern boundary. These maxima are located at the depth of 1800 m. The highest vertical speed, $\sim -1 \times 10^{-4} \text{ m s}^{-1}$, in the domain occurs along the eastern boundary to the south of $\Phi = 25^\circ\text{S}$ at the depth of about 700 m. To the north of it, there is strong upwelling, $\sim 0.5 \times 10^{-4} \text{ m s}^{-1}$, at the depth of about 2000 m. This pattern of up- and downwelling is very similar to that found in Sugimoto and Aoki (1991). For the upcurrent experiment, the pattern is quite similar, but the speed maxima along the western and eastern boundaries are twice those of the centered experiment and the maximum along the southern boundary is 20% larger than that in the centered experiment.

The deep temperature is higher by about 1.2°C below the main thermocline in the upcurrent case than in the centered case. This is most likely due to computational diffusion in the upcurrent scheme.

For the centered-difference experiment, the strong up- and downwelling give a grid Péclet number of ~ 200 at the vertical speed maxima mentioned above, and generally ≥ 20 along the lateral boundaries to the south of 10°S . An instance of artificial convective adjustment is found at depths 1000–2000 m and $20^\circ-15^\circ\text{S}$ along the eastern boundary. Here we identify artificial convection as convection that begins from a middepth. Global effects of this numerical instability, however, are negligibly small: the density overshoots created by numerical instability are very small and associated artificial convective adjustment penetrates only a few grid points downward. This is because instability occurs in the present configuration only where the density stratification is very weak owing to the deep convection that occurs in the southern hemisphere to produce the deep water.

This is in contrast to the body-cooling case, where the body cooling maintains a relatively sharp thermocline at 1000-m depths. Upwelling along the western boundary in the southern hemisphere crosses the thermocline and produces large density overshoots and artificial convection in the centered-difference case. To summarize, if there is strong upwelling crossing a strong stratification, there can be artificial convection that creates a significant density signal but, if the

stratification is weak, the signal is also weak even with strong upwelling.

3. World Ocean

a. Model and experimental design

In this section, we use a World Ocean general circulation model with a realistic topography. The model configuration and parameters are described in detail by [Hasumi and Suginohara \(1999\)](#). The ocean is forced only at the sea surface. The wind stress is the monthly climatology of [Hellerman and Rosenstein \(1983\)](#), and the sea surface temperature and salinity are restored to the monthly climatologies of [Levitus and Boyer \(1994\)](#) and [Levitus et al. \(1994\)](#), respectively. The restoring time is 30 days for both temperature and salinity. Isopycnal diffusion ([Cox 1987](#)) is used, where the isopycnal diffusivity and background horizontal diffusivity are $1 \times 10^3 \text{ m}^2 \text{ s}^{-1}$ and $1 \times 10^2 \text{ m}^2 \text{ s}^{-1}$ respectively. The vertical eddy diffusivity is $0.5 \times 10^{-4} \text{ m}^2 \text{ s}^{-1}$. The horizontal resolution is taken to be $2.8^\circ \times 2.8^\circ$. There are 40 levels in the vertical with resolution increasing from 50 m at the sea surface to 200 m near the bottom. We conduct two experiments ([Table 1](#)) with the centered difference scheme (expt IV) and the weighted upcurrent scheme (expt V). The weight of the upcurrent scheme is $\alpha = 0.7$ in the horizontal and $\alpha = 0.97$ in the vertical. We use convective adjustment for both cases, where the standard convection scheme of the CCSR-OGCM ([Hasumi and Suginohara 1995](#)) is employed. In each experiment, the model is integrated from a state of no motion and horizontally uniform temperature and salinity distribution for 5500 years, and the final state is nearly an equilibrium annual cycle. We discuss the annual mean field of the final year.

b. Results and discussion

[Figure 3](#) shows the meridional volume transport streamfunction for the Pacific, and the meridional sections of the temperature and grid Péclet number along 170°W . In the centered difference case (expt IV), the grid Péclet number is large from the sea surface to the depth of 200 m at the equator ([Fig. 3c](#)), and the streamfunction contours show unusual bends at 200 m at latitudes 5°S and 5°N ([Fig. 3a](#)). As will be seen shortly, this feature is most likely due to numerical instability and resultant artificial convective adjustment associated with Ekman upwelling and downwelling. The grid Péclet number is also very large in the Southern Ocean and over irregular bottom topography.


[Figure 4](#) shows the frequency of convective adjustment occurrence and the grid Péclet number in expts IV and V. In the centered difference case (expt IV), convection occurs at the depth of 125 m in the east equatorial Pacific. The grid Péclet number is very large there ([Fig. 4b](#)). This convection is of course artificial. The most intense part of the convection reaches the depth of 250 m (not shown). This is perhaps the cause of the bends of the overturning streamfunction mentioned earlier ([Fig. 3a](#)). These artificial features are much more pronounced in one of [Hasumi and Suginohara's \(1999\)](#) experiments, designated CTDIFF, with the centered scheme. The only difference between their experiment CTDIFF and our experiment IV is that the vertical eddy diffusivity is $A_{\text{HV}} = 0.1 \times 10^{-4} \text{ m}^2 \text{ s}^{-1}$ for CTDIFF while it is $0.5 \times 10^{-4} \text{ m}^2 \text{ s}^{-1}$ for our expt IV. They find artificial features not only in the equatorial regions but also at other latitudes.

Y. Yamanaka (1999 personal communication) shows that the “nutrient trapping” ([Najjar et al. 1992](#)), a well-known artificial maximum of nutrients appearing near the equator in biogeochemical general circulation models, is greatly reduced when the weighted upcurrent scheme is used. [Oschlies \(1999\)](#), manuscript submitted to *Global Biogeochem. Cycles* obtains similar results. They both indicate that numerical instability or dispersion associated with strong equatorial upwelling is one of the causes for the nutrient trapping.

Instances of artificial convective adjustment are also found (not shown) in the Weddell Sea and Greenland Sea and off the southern coast of Greenland, where very strong vertical velocity ($\sim 0.5 \times 10^{-4} \text{ m s}^{-1}$) occurs. These convections, however, do not seem to have a global effect because the stratification is very weak at those locations and tracer anomalies created by the instability are negligibly small.

[Hasumi and Suginohara \(1999\)](#) run almost the same experiment with the same vertical eddy diffusivity ($A_{\text{HV}} = 0.5 \times 10^{-4} \text{ m}^2 \text{ s}^{-1}$) as ours except that they use the UTOPIA/QUICKEST scheme for tracer advection. This experiment is designated UTOPIA-5. We find that the temperature of the deep Pacific water to the north of 30°S is $0.1^\circ\text{--}0.2^\circ\text{C}$ lower in our expt IV than that in their experiment UTOPIA-5. Since numerical instability and associated artificial convection are unlikely to be the cause for this difference, as mentioned above, it may be that the difference between the advection term evaluated with the centered scheme and that with the UTOPIA/QUICKEST scheme itself causes the difference in deep temperature.

In the weighted upcurrent case (expt V), the vertical temperature distribution is much more diffuse from the sea surface to the bottom than that of the centered difference counterpart (compare [Figs. 3b and 3e](#)). The temperature of the Pacific

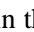
deep water is 0.8°–1.2°C higher than that of [Hasumi and Sugimoto's \(1999\)](#) UTOPIA-5. This is due to computational diffusion. Since this enhanced diffusivity transports more heat into the deep water, the meridional overturning is stronger (cf. [Figs. 3a and 3d](#) ).

We have examined effects of numerical instability and large computational diffusion in our 40-level model. The vertical resolution of this model is high compared with that of typical coarse-resolution World Ocean GCMs (e.g., [Large et al. 1997](#); [Mikolajewicz and Crowley 1997](#)), whose level thicknesses are typically 400–1000 m below the depth of 2000 m. The problems of these classical advection schemes must therefore appear also in other models. For example, the convection at 10°S and 10°N in the equatorial Pacific in [Toggweiler et al.'s \(1989\)](#) model is probably caused by numerical instability associated with Ekman downwelling (see their Figs. 6 and 7).

Higher modes are enhanced at the equator in these World Ocean simulations, and, for example, there are an eastward flow of $\sim 0.5 \text{ cm s}^{-1}$ near the bottom ($\sim 4500 \text{ m}$) and a westward flow of $\sim 0.1 \text{ cm s}^{-1}$ at the depth of about 4000 m from 150°W to 130°W in both experiments IV and V (not shown). However, it is not clear whether this feature is really a manifestation of the zonal jets appearing in the idealized basin discussed in the preceding section or other kind of flows controlled by bottom topography.

4. Summary

We have compared two classical advection schemes, the centered difference and weighted upcurrent, using OGCMs with an idealized basin and a realistic World Ocean topography. We have also shown the results of a super-high vertical resolution model of 800 levels for the idealized basin, where the grid Péclet number criterion is perfectly satisfied.

Stacked jets are found along the equator in the idealized-basin models of both low- and super-high resolutions. This shows that numerical instability is not necessary for the existence of the stacked jets. The balance of the terms in the temperature (density) equation suggests that the jets are maintained by horizontal diffusion, as concluded by [Wang \(1995\)](#). We have also used a 5-level OGCM for the same idealized basin with the centered difference and weighted upcurrent schemes (not shown). This model is a variation on the 12-level body-cooling one discussed in [section 2](#), and the only difference is the vertical grid spacing: 400, 500, 880, 1000, and 1220 m from the sea surface to the bottom. In the centered difference case, the amplitude of the stacked jets is extremely large, the maximum zonal-mean zonal velocity near the equator being 1 cm s^{-1} , while the jets in the weighted upcurrent case, with maximum zonal-mean zonal velocity of about 0.25 cm s^{-1} , is not so different from those of the 800-level model. In the 5-level centered case, there are instances of artificial convective adjustment all along the western boundary in the southern hemisphere, which suggests strong numerical instability. The balance of the density terms to the south of the core of the eastward jet, however, is again mainly between horizontal diffusion and vertical advection terms in the 5-level centered difference case as in the 800-level case ([Fig. 2](#) ). This suggests that the stacked jets are a kind of equatorial boundary layer, like that of [Kawase \(1987\)](#), and that the boundary layer solution is “intrinsic”; that is, the solution is always there but how strongly it is excited depends on other conditions outside the boundary layer. The agent that excites the jets may vary. In our 5-level centered difference case, it seems that the numerical instability along the western boundary strongly excites the equatorial jets. [Weaver and Sarachik \(1990\)](#) report that numerical instability near the eastern boundary seems to be the cause of the jets. In the “true” solution of our super-high resolution model, the agent is something other than numerical instability.

[Kawase's \(1987\)](#) solution is made possible by diapycnal mixing due to vertical diffusion, while the stacked jets in our OGCMs seem to be due to horizontal diffusion. In [Tsujino's \(1998\)](#) idealized two-basin model, where he uses a high accuracy advection scheme with small computational diffusion and computational dispersion ([Hasumi and Sugimoto 1999](#)), isopycnal diffusion plus small background horizontal diffusion to minimize diapycnal mixing arising from horizontal diffusion, and a large vertical diffusivity ($\sim 3 \times 10^{-4} \text{ m}^2 \text{ s}^{-1}$) in the deep, there are stacked jets, which seem to be maintained mainly by vertical diffusion. This suggests that equatorial stacked jets can exist as long as there is a mechanism of sufficient diapycnal mixing. Whether or not there is actually sufficient mixing in the real ocean is an open question. Observations show that there are vertically alternating zonal flows in the equatorial deep Pacific ([Firing 1989](#); [Johnson and Toole 1993](#)). We do not, however, have data enough to determine whether these flows are “stacked jets” found in OGCMs or not.

Using the result of the 800-level model as a reference, we have found the following characteristics of the two advection schemes as applied to a thermally forced box ocean. The centered difference scheme, in places where strong vertical motion crosses strong stratification, tends to lead to density overshoots and consequential artificial convective adjustment, which makes the deep density higher than that of the “true solution,” the solution of the 800-level model. On the other hand, computational diffusion associated with the weighted upcurrent scheme causes a more diffuse thermocline and less dense deep water.

These characteristics of the two schemes also apply to the World Ocean models. Ekman upwelling and downwelling, which are absent in the idealized-basin experiments, result in a large grid Péclet number: with the centered scheme,

numerical instability and ensuing artificial convective adjustment in the equatorial Pacific cause an unrealistic circulation there, although artificial convection in the Greenland Sea and Weddell Sea has little global effect because the vertical temperature and salinity stratification is very weak there. The weighed upcurrent scheme leads to a warmer deep water and more diffuse thermocline. Both advection schemes thus have merits and pitfalls.

To avoid the pitfalls, we need either to increase the vertical resolution or to use a better advection scheme. Necessary vertical resolution to satisfy the Péclet number criterion in most of the world ocean domain with a vertical eddy diffusivity of $\sim 0.5 \times 10^{-4} \text{ m}^2 \text{ s}^{-1}$ will be less than 100 m below the depth of 3000 m and less than 20 m above 1000 m. Even with such resolution, however, effects of numerical dispersion associated with the centered scheme will be significant near the surface in the equatorial region ([Oschlies 2000](#)). In addition, with a more realistic value of vertical eddy diffusivity, $\sim 0.1 \times 10^{-4} \text{ m}^2 \text{ s}^{-1}$, in the main thermocline problems with the centered scheme will be more serious ([Hasumi and Suginohara 1999](#)).

It is therefore desired that efficient and accurate advection schemes such as MPDATA ([Smolarkiewicz 1984](#)) and UTOPIA/QUICKEST ([Leonard et al. 1993](#)) be incorporated into OGCMs. Comparison of these schemes with the centered difference scheme is found in the companion paper, [Hasumi and Suginohara \(1999\)](#).

Acknowledgments

We would like to thank Kirk Bryan for fruitful discussions. Thanks are extend to Syukuro Manabe, Tertia Hughes, and Robbie Toggweiler for helpful discussions and comments. Constructive comments from two anonymous reviewers helped substantially improve the manuscript. Numerical calculations were performed on HITAC S3800 and SR8000 at the Computer Centre of the University of Tokyo. Some of the figures were produced with GrADS (<http://grads.iges.org/grads/head.html>), and the others with the GFD-Dennou Libraries (<http://www.gfd-dennou.org/>).

REFERENCES

- Bacastow, R., and E. Maier-Reimer, 1990: Ocean-circulation model of the carbon cycle. *Climate Dyn.*, **4**, 95–125.
- Bryan, K., 1989: The design of numerical models of the ocean circulation. *Ocean Circulation Models: Combining Data and Dynamics*, D. L. T. Anderson and J. Willebrand, Eds., Kluwer Academic, 465–500.
- Cox, M. D., 1987: Isopycnal diffusion in a z-coordinate ocean model. *Ocean Modelling* (unpublished manuscripts), **74**, 1–5.
- Firing, E., 1989: Mean zonal currents below 1500 m near the equator, 159°W. *J. Geophys. Res.*, **94**, 2023–2028.
- Furue, R., K. Nakajima, and I. Ishikawa, 1995: Modal decomposition of deep ocean circulation models: Comparison with reduced-gravity models. *J. Geophys. Res.*, **100**, 10567–10588.
- Hasumi, H., and N. Suginohara, 1995: Haline circulation induced by formation and melting of sea ice. *J. Geophys. Res.*, **100**, 20613–20625.
- , and —, 1999: Sensitivity of a global ocean general circulation model to tracer advection schemes. *J. Phys. Oceanogr.*, **29**, 2730–2740.
- Hellerman, S., and M. Rosenstein, 1983: Normal monthly wind stress over the world ocean with error estimates. *J. Phys. Oceanogr.*, **13**, 1093–1104.
- Ishikawa, I., S. Aoki, R. Furue, and N. Suginohara, 1996: Convection induced by cooling at one side wall in two-dimensional non-rotating fluid: Applicability to the deep Pacific circulation. *J. Oceanogr.*, **52**, 617–632.
- Johnson, G. C., and J. M. Toole, 1993: Flow of deep and bottom waters in the Pacific at 10°N. *Deep-Sea Res.*, **40**, 371–394.
- Kawase, M., 1987: Establishment of deep ocean circulation driven by deep-water production. *J. Phys. Oceanogr.*, **17**, 2294–2317.
- Large, W. G., G. Danabasoglu, S. C. Doney, and J. C. McWilliams, 1997: Sensitivity to surface forcing and boundary layer mixing in a global ocean model: Annual-mean climatology. *J. Phys. Oceanogr.*, **27**, 2418–2447.
- Leonard, B. P., M. K. MacVean, and A. P. Lock, 1993: Positivity-preserving numerical schemes for multidimensional advection. NASA TM106055, ICOMP-93-05, Lewis Research Center, 62 pp. [Available from National Aeronautics and Space Administration, Washington, DC 20546-0001.].
- Levitus, S., and T. P. Boyer, 1994: *World Ocean Atlas 1994*. Vol. 4; *Temperature*, U.S. Department of Commerce, Washington, DC, 117

— R. Burgett, and T. P. Boyer, 1994: *World Ocean Atlas 1994*. Vol 3; *Salinity*, U.S. Department of Commerce, Washington, DC, 99 pp.

Maier-Reimer, E., U. Mikolajewicz, and K. Hasselmann, 1993: Mean circulation of the Hamburg LSG OGCM and its sensitivity to the thermohaline surface forcing. *J. Phys. Oceanogr.*, **23**, 731–757.

Mikolajewicz, U., and T. J. Crowley, 1997: Response of a coupled ocean/energy balance model to restricted flow through the central American isthmus. *Paleoceanography*, **12**, 429–441.

Najjar, R. G., J. L. Sarmiento, and J. R. Toggweiler, 1992: Downward transport and fate of organic matter in the ocean: Simulations with a general circulation model. *Global Biogeochem. Cycles*, **6**, 45–76.

Obata, A., R. Furue, S. Aoki, and N. Suginohara, 1996: Modeling layered structure in deep Pacific circulation. *J. Geophys. Res.*, **101**, 3663–3674.

Oschlies, A., 2000: An unrealistic high-salinity tongue simulated in the tropical Atlantic: Another example illustrating the need for a more careful treatment of vertical discretizations in OGCMs. *Ocean Modelling*, in press.

Pacanowski, R. C., 1995: MOM 2 documentation, user's guide and reference manual. GFDL Ocean Tech. Rep. 3, Geophysical Fluid Dynamics Laboratory, Princeton, NJ, 232 pp. [Available from GFDL, Princeton, NJ 08542-0308.].

Rood, R. B., 1987: Numerical advection algorithms and their role in atmospheric transport and chemistry models. *Rev. Geophys.*, **25**, 71–100.

Smolarkiewicz, P. K., 1984: A fully multidimensional positive definite advection transport algorithm with small implicit diffusion. *J. Comput. Phys.*, **54**, 325–362.

Stommel, H., and A. B. Arons, 1960: On the abyssal circulation of the world ocean—II. An idealized model of the circulation pattern and amplitude in oceanic basins. *Deep-Sea Res.*, **6**, 217–233.

Suginohara, N., and M. Fukasawa, 1988: Set-up of deep circulation in multi-level numerical models. *J. Oceanogr. Soc. Japan*, **44**, 315–336.

— and S. Aoki, 1991: Buoyancy-driven circulation as horizontal convection on a β -plane. *J. Mar. Res.*, **49**, 295–320.

— — and M. Fukasawa, 1991: Comments on “On the importance of vertical resolution in certain oceanic general circulation models.” *J. Phys. Oceanogr.*, **21**, 1699–1701.

Toggweiler, J. R., K. Dixon, and K. Bryan, 1989: Simulations of radiocarbon in a coarse-resolution world ocean model, 1, Steady state prebomb distributions. *J. Geophys. Res.*, **94**, 8217–8242.

Tsujino, H., 1998: Modelling study on thermohaline circulation in the Pacific Ocean. Ph.D. thesis, University of Tokyo, 110 pp.

Wang, D., 1995: On thermally forced deep equatorial circulation in a GCM. *J. Phys. Oceanogr.*, **25**, 2155–2165.

Weaver, A. J., and E. S. Sarachik, 1990: On the importance of vertical resolution in certain ocean general circulation models. *J. Phys. Oceanogr.*, **20**, 600–609.

— and — 1991: Reply. *J. Phys. Oceanogr.*, **21**, 1702–1707.

Yamanaka, Y., and E. Tajika, 1996: The role of the vertical fluxes of particulate organic matter and calcite in the oceanic carbon cycle: Studies using an ocean biogeochemical general circulation model. *Global Biogeochem. Cycles*, **10**, 361–382.

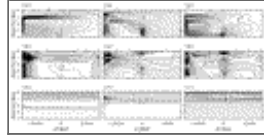
Tables

Table 1. List of experiments

Expt	Basin	Vertical levels	Advection scheme
I	Idealized	800	Centered difference
II	Idealized	12	Centered difference
III	Idealized	12	Weighted upcurrent
IV	Realistic world ocean	40	Centered difference
V	Realistic world ocean	40	Weighted upcurrent

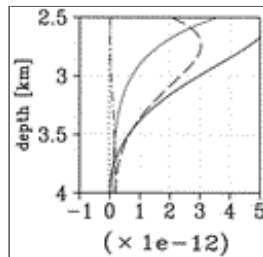
[Click on thumbnail for full-sized image.](#)

Figures



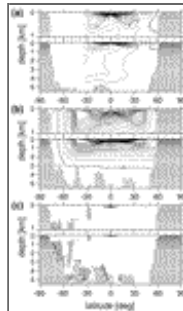
[Click on thumbnail for full-sized image.](#)

Fig. 1. (a) Zonally integrated volume transport streamfunction for expt I; the contour interval (CI) is 0.5 Sv. (b) Zonally averaged zonal velocity for expt I; CI is 0.05 cm s^{-1} . (c) Zonally averaged density for expt I; the interval between the solid contours is $0.2 \sigma_\theta$, and the dashed contours are drawn from $2.99 \sigma_\theta$ at the interval of $0.001 \sigma_\theta$. Also plotted are the differences of expt II from expt I (d) in the zonally integrated volume transport streamfunction (CI = 0.2 Sv), (e) in the zonally averaged zonal velocity (CI = 0.03 cm s^{-1}), and (f) in the zonally averaged density (CI = $0.025 \sigma_\theta$). (g), (h), and (i) are respectively the same as (d), (e), and (f) but for the differences of expt III from expt I. The shaded areas in the streamfunctions indicate clockwise circulation; those in the zonal velocity maps, westward velocity; and those in the density difference maps, negative values. To compute the difference of a 12-level model (expt II or III) from the 800-level model, we first construct a 12-level dataset from the 800-level model variable by averaging it within the depth range of the corresponding single level of the 12-level model



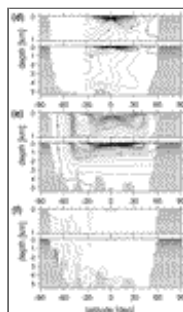
[Click on thumbnail for full-sized image.](#)

Fig. 2. Balance in the density equation for expt I at $x = 1450 \text{ km}$, $y = -50 \text{ km}$ (the closest density point to the equator). The unit of the abscissa is $\sigma_\theta \text{ s}^{-1}$. Solid line: $-w\rho_z$. Long-dashed line: $-A_{HH}\rho_{yy}$. Short-dashed line: $-A_{HV}\rho_{zz}$. Dash-dotted line: $-u\rho_x$. The other terms are much smaller in magnitude than the above four and are all plotted with thin dotted lines



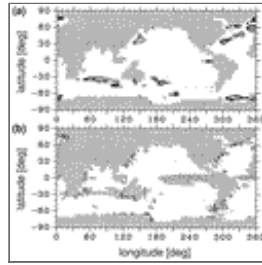
[Click on thumbnail for full-sized image.](#)

Fig. 3. (a) Zonally integrated volume transport streamfunction for the Pacific for expt IV. The contour interval (CI) is 2 Sv. The dashed contours indicate clockwise circulation. (b) Temperature along 170°W for experiment IV. CI = 1°C . (c) Grid Péclet number along 170°W for experiment IV. The contour levels are logarithmically spaced: 1, 2, 4, 8, 16, 32, 64, and 128. The dark shading indicates values larger than unity



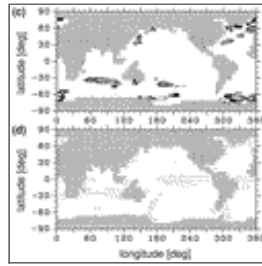
[Click on thumbnail for full-sized image.](#)

Fig. 3. (Continued) Panels (d), (e), and (f) are respectively the same as (a), (b), and (c) but for expt V. In (f), the light shading with a dotted boundary indicates regions where the computational diffusion is larger than the specified one. From the formulas (2) and (3), we can see that $A_{\text{comp}}/A_{\text{HV}} = \text{Pe} \times (\alpha - 0.5)/(1 - \alpha) \approx \text{Pe} \times 16$, that is, the ratio of the computational diffusion coefficient to the specified diffusion coefficient can be obtained by multiplying Pe by about 16



[Click on thumbnail for full-sized image.](#)

Fig. 4. (a) Frequency of the occurrence of convective adjustment at the depth of 125 m and (b) the grid Péclet number at 100 m in expt IV. Panels (c) and (d) are the same as (a) and (b) but for expt V. The frequency indicates, in terms of percentage, how often convective adjustment occurs during the last year of the model integration; the contour interval is 5%



[Click on thumbnail for full-sized image.](#)

Fig. 4. (Continued) The contour levels for the grid Péclet number are 1, 2, 4, 16, 32, 64, and 128; the dark shading indicates values larger than unity. In (d), the light shading with a dotted boundary indicates regions where the computational diffusion is larger than the specified one

* Current affiliation: Graduate School of Environmental Earth Science, Hokkaido University, Sapporo, Japan.

Corresponding author address: Dr. Ryo Furue, Center for Climate System Research, University of Tokyo, 4-6-1 Komaba, Meguro-ku, Tokyo 153-8904, Japan.

E-mail: furufuru&commat.sr.u-tokyo.ac.jp

[top ▲](#)



© 2008 American Meteorological Society [Privacy Policy and Disclaimer](#)
 Headquarters: 45 Beacon Street Boston, MA 02108-3693
 DC Office: 1120 G Street, NW, Suite 800 Washington DC, 20005-3826
amsinfo@ametsoc.org Phone: 617-227-2425 Fax: 617-742-8718
[Allen Press, Inc.](#) assists in the online publication of AMS journals.